

# High-rate quantum LDPC codes for long-range-connected neutral atom registers

Laura Pecorari,<sup>1</sup> Sven Jandura,<sup>1</sup> Gavin K. Brennen,<sup>2</sup> and Guido Pupillo<sup>1</sup>

<sup>1</sup>*University of Strasbourg and CNRS, CESQ and ISIS (UMR 7006), aQCESS, 67000 Strasbourg, France*

<sup>2</sup>*Center for Engineered Quantum Systems, School of Mathematical and Physical Sciences, Macquarie University, 2109 NSW, Australia*

(Dated: April 22, 2024)

High-rate quantum error correcting (QEC) codes with moderate overheads in qubit number and control complexity are highly desirable for achieving fault-tolerant quantum computing. Recently, quantum error correction has experienced significant progress both in code development and experimental realizations, with neutral atom qubit architecture rapidly establishing itself as a leading platform in the field. Scalable quantum computing will require processing with QEC codes that have low qubit overhead and large error suppression, and while such codes do exist, they involve a degree of non-locality that has yet to be integrated into experimental platforms. In this work, we analyze a family of high-rate Low-Density Parity-Check (LDPC) codes with limited long-range interactions and outline a near-term implementation in neutral atom registers. By means of circuit-level simulations, we find that these codes outperform surface codes in all respects when the two-qubit nearest neighbour gate error probability is below  $\sim 0.1\%$ . We show how these codes can be natively integrated in two-dimensional static neutral atom qubit architectures with open boundaries, where the desired long-range connectivity can be targeted via Rydberg-blockade interaction. Our protocol solely requires multiple laser colors to enable transitions to different Rydberg states for different interatomic distances.

Since Kitaev’s seminal works [1, 2], the surface code has been the dominant choice for quantum error correction (QEC) as its set of check operators, or stabilizers, is simple and geometrically local enabling parallel syndrome extraction with a high tolerance to errors. However, the encoding – only one logical qubit per code independently of the size – is poor, posing a large resource overhead for scalable quantum computing. The surface code is but one example of a broader class of Low-Density Parity-Check (LDPC) codes [3, 4], other members of which retain all the good properties of the surface code such as large distance, which quantifies the number of correctable errors, while allowing for more favourable encoding rates, defined by the ratio of logical qubits to physical qubits.

Recently, there has been intense activity benchmarking the performance of various LDPC codes both for fault-tolerant error correction [5] and quantum computing [6] with the results converging towards the idea that “*the more non-local, the better*”. However, relatively little investigation has been made into how to use the physics available natively in quantum computing platforms to maximally utilize the advantages of these codes (for an example of such see Ref. [7]). In this work we analyze a family of high-rate quantum LDPC codes built via hypergraph product (HGP) construction [8–11]. We refer to them as *La-cross codes*, since the arrays of their stabilizer shapes, each consisting of a surface code stabilizer cross with two extra long-range interactions, is reminiscent of a long-armed cross stitch pattern (Fig. 1(a)). The length of these interactions – or amount of non-locality – solely depends on the parameters of the classical seeds the quantum code is constructed from and thus is, to an extent, tunable. We discuss encoding capabilities and

probe tolerance to errors via circuit-level simulations accounting for state preparation, measurement, single- and range-dependent two-qubit gate errors. Compared to the surface code with same number of physical and logical qubits, we obtain sub-threshold logical error probability reductions that can reach order of magnitude and increase with the number of physical qubits. The second part of this work is aimed at making contact with near-term experiments with neutral atom quantum registers [12–17]. For two-dimensional arrays with open boundaries, we show how the Rydberg blockade mechanism enables the necessary long-range gates for stabilizer measurements without need for swapping or qubit shuttling. Our error model accounts for fidelity decay as a function of gate distance, due fundamentally to the decay of the van der Waals interaction strength.

Finally, we show further improvement by adopting an error model with range-independent gate errors. In this case, the threshold increases and the onset of improvement over the surface code occurs at higher physical error probabilities. For example, the most non-local instance of La-cross codes discussed in this work shows improvement over the surface code below nearest neighbour gate error probabilities of  $\sim 0.5\%$ , already outperforming the surface code logical failure probability by more than one order of magnitude at physical error probabilities of  $\sim 0.1\%$ . Such a range-independent noise model may be realized by qubit shuttling in neutral atom registers [7, 18], or in different physical platforms like photonic registers with direct non-local fibre coupling [19] or matter-based qubit architectures with cavity-mediated interactions [20].

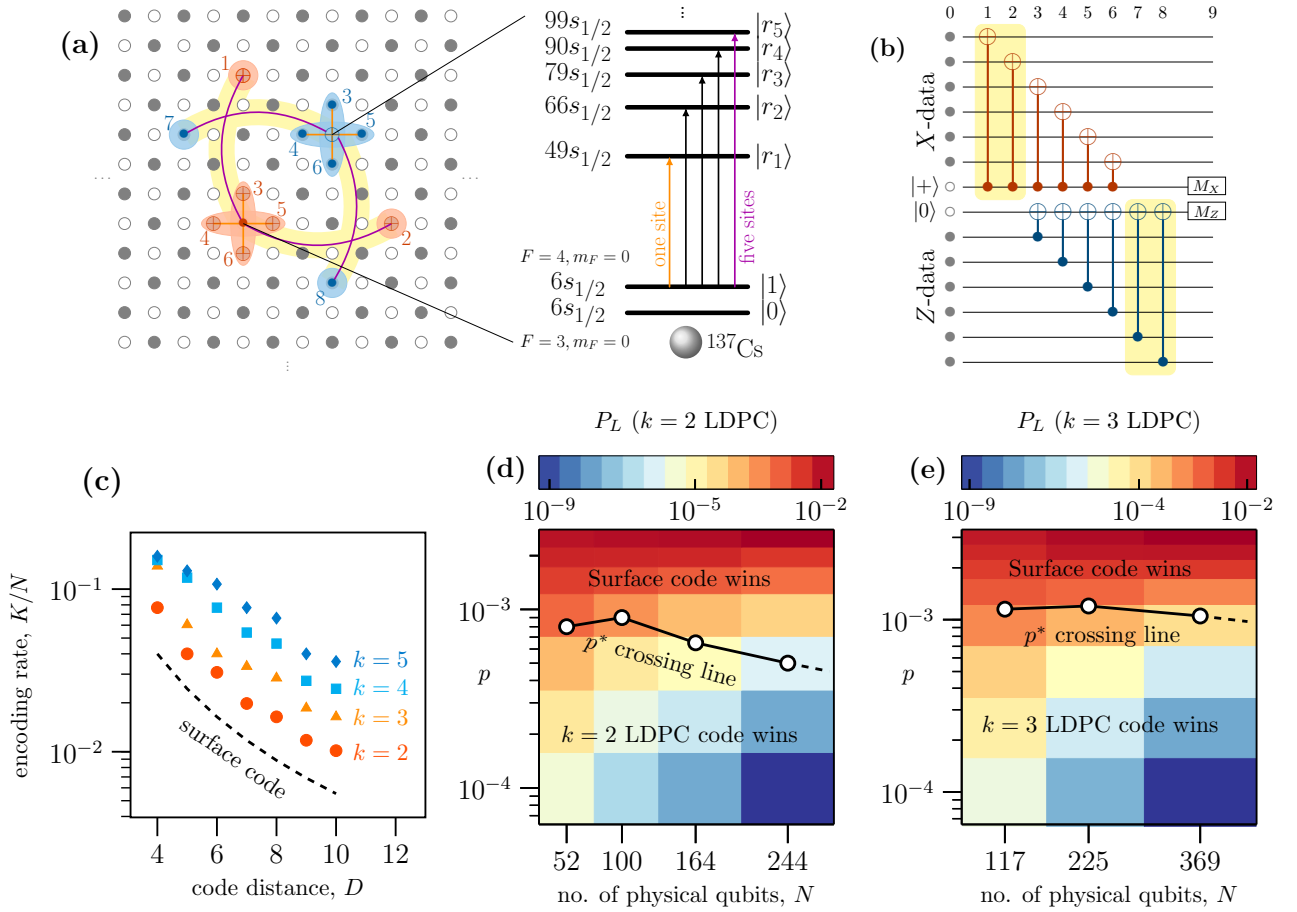


FIG. 1. (a) Array patch with data (gray) and ancillary (white) qubits hosting one instance of the here analyzed LDPC code family. Long-range interactions are highlighted in yellow, two stabilizers are drawn (red and blue) with displayed CNOT measurement order for syndrome extraction. The inset shows energy levels and selected transitions (vertical arrows) to different Rydberg states for implementation with neutral atom qubits. Two-qubit gates between one and five lattice sites separated qubits and corresponding Rydberg transitions are coloured in orange and violet, respectively. Principal quantum numbers are chosen to minimize gate infidelity while still preserving a sufficient Rydberg blockade strength (see text). (b) Depth-10 syndrome measurement circuit neglecting idle errors. (c) Encoding rate, hence qubit overhead, comparison between  $k$ -LDPC codes and surface code (SC) given the same number of logical qubits and code distance. (d)-(e) Illustration showing logical failure probability for  $k = 2$ - and  $3$ -LDPC codes as a function of nearest neighbour two-qubit gate physical error probability and number of physical qubits. Solid lines correspond to crossing probabilities below which the LDPC logical error probability gets lower than the surface code one, assuming equal number of logical and physical qubits for both codes. Dashed black line is extrapolation to larger numbers of physical qubits.

## RESULTS

### Quantum LDPC codes

Quantum LDPC codes [3] are stabilizer codes where both the number of qubits acted on by each stabilizer and the number of stabilizers acting on each qubit are constantly bounded. Their parity check matrix is then sparse, hence the notion of *low density* invoked in their name. Their encoding rate satisfies  $K/N \xrightarrow{N \rightarrow \infty} C \geq 0$ , for some constant  $C$ , being  $N$  and  $K$  the number of physical and logical qubits, respectively. While constant rate,

$C > 0$ , quantum LDPC codes exist, the better studied examples have zero rate. The surface code is an example with  $K = \mathcal{O}(1)$ , hence zero rate, and a code distance  $D = \mathcal{O}(\sqrt{N})$ . For practical use, it is not necessarily the asymptotic scaling of the rate that matters, but rather choosing a code with a favorable ratio  $K/N$  for large but finite  $N$ , together with a large distance.

In the following we review how a quantum LDPC code can be constructed by combining two classical LDPC codes via hypergraph product construction. The hypergraph product (HGP) [8] starts from two classical linear codes  $\mathcal{C}_i = [n_i, k_i, d_i]$  encoding  $k_i$  logical bits in  $n_i$

physical bits ( $i = 1, 2$ ). The codewords words of these classical codes are the kernel of the *parity check matrix*  $H_i \in \mathbb{F}_2^{r_i \times n_i}$ , where  $r_i$  is the number of checks, giving  $k_i = n_i - \text{rank}(H_i)$  encoded bits. The minimal Hamming distance between two codewords is called the distance  $d_i$ . Associated with each classical code is a *transposed code*  $\mathcal{C}_i^T = [r_i, k_i^T, d_i^T]$  with parity matrix  $H_i^T$ . The HGP construction now combines the two classical codes to a  $[[N, K, D]]$  quantum quantum stabilizer code of Calderbank-Shor-Steane type with quantum parity check matrix

$$H_q = \left( \begin{array}{cc|cc} 0 & 0 & H_1 \otimes \mathbb{I}_{n_2} & \mathbb{I}_{r_1} \otimes H_2^T \\ \mathbb{I}_{n_1} \otimes H_2 & H_1^T \otimes \mathbb{I}_{r_2} & 0 & 0 \end{array} \right).$$

where  $N = n_1 n_2 + r_1 r_2$  is the number of physical qubits and  $K = k_1 k_2 + k_1^T k_2^T$  is the number of encoded logical qubits. The first  $n_1 r_2$  rows of  $H_q$  describe the  $X$  stabilizers of the CSS code, the following  $n_2 r_1$  rows describe the  $Z$  stabilizers. The *distance*  $D$  of this quantum code denotes the minimum weight of a Pauli operator commuting with all stabilizers. It can be shown that for the HGP construction the distance satisfies  $D \geq \min\{d_1, d_2, d_1^T, d_2^T\}$ .

For the present purposes, we have chosen the seed codes  $\mathcal{C}_i$  to be cyclic codes generalizing the repetition code the surface code is built upon. Such a choice both allows for improving the encoding rate and retaining most of the intuitiveness of the surface code, at the price of a non-constant overhead in the asymptotic limit. However, this does not represent a severe issue in the prospect of implementation on near-term quantum computers, as we will discuss more quantitatively in the next sections.

### Classical seeds constrain quantum layout

In this section we review how the stabilizers, logical operators, and array shape of a quantum HGP code are determined from its classical seeds. This represents a huge help in designing new LDPC codes tailored to the connectivity of the quantum hardware.

We have chosen cyclic seed codes, i.e. codes with cyclic shift invariant codewords. If their parity check matrix,  $H$ , is circulant, i.e. a square matrix whose rows are cyclic shifts of the first row [10], the code is fully specified by the first row of  $H = \text{circ}(c_0, c_2, \dots, c_k, 0, \dots, 0) \in \mathbb{F}_2^{n \times n}$ , whose entries — for the sake of representation — can be mapped to the coefficients of a degree- $k$  polynomial in the form  $h(x) = 1 + \sum_{i=1}^k c_i x^i$ . More formally, we say that there exists an isomorphism  $\mathbb{F}_2^n \rightarrow \mathbb{F}_2[x]/(x^n - 1)$  mapping cyclic linear codes  $\mathcal{C} \subseteq \mathbb{F}_2^n$  into polynomials with coefficients in  $\mathbb{F}_2$  dividing  $x^n - 1$  modulo 2, being  $n$  the number of bits of the code. Building blocks of length- $n$  cyclic codes correspond to factors of  $x^n - 1$ . For  $k = 1$  the repetition code is recovered.

We note that there always exists a mapping from quantum parity check matrix to array indexing so that the shape of the stabilizers of the code can be directly inferred from the polynomial of the classical seed, see Fig. 2(a). Additionally, there always exists a basis where logical operators align along the same row or column. In contrast to the surface code where logical operators are Pauli strings stretching from boundary to boundary, for this code family logical operators are Pauli strings — possibly with holes — which are shorter in length and larger in number (Fig. 2(b)). As a second remark, we observe that, if  $H$  is circulant, for any  $n$  only some  $k$ 's are allowed, as  $H$  may happen to be full rank, and thus  $k = 0$ . The HGP of equal seeds having circulant parity check matrix,  $H \in \mathbb{F}_2^{n \times n}$ , naturally leads to a quantum code with periodic boundary conditions and parameters  $N = 2n^2$ ,  $K = 2k^2$ . In this work we are interested in codes with open boundary conditions for the sake of experimental realization, thus we choose  $H \in \mathbb{F}_2^{(n-k) \times n}$ , which by being rectangular allows for any choice of  $k$  and  $n$ . Quantum parameters now read  $N = (n-k)^2 + n^2$  and  $K = k^2$  (half logical qubits get “lost”), with consequent array shape shown in Fig. 2(c), which can be squeezed to restore the square configuration. As a consequent effect, squeezed stabilizers allow for effectively shorter, hence higher-fidelity, gates.

In the following we stick to a sub-family of HGP codes with equal seed polynomials of the form  $h(x) = 1 + x + x^k$  and consequently weight-6 stabilizers which we study for different values of  $k$ . The  $k = 2$  instance of this family has recently been studied in [18], where the possibility of implementation via qubit shuttling is discussed. This polynomial choice provides quantum codes with high rate, low stabilizer weight and moderate non-locality both in terms of *range* and *number* of long-range, while allowing for a similar implementation scheme as the surface code. We mention in passing that the similar polynomial  $\bar{h}(x) = 1 + x^k$  leads to codes with a shorter distance than  $h(x) = 1 + x + x^k$  and shows no apparent improvement in the overhead over the surface code. For example, the HGP of two  $[9, 3, 3]$  classical codes, i.e.  $1 + x^3$ , leads to a quantum code with  $N = 162$  (periodic boundary conditions) or  $N = 117$  (open boundary conditions). These code parameters exactly match the number of physical qubits of  $K$  copies of surface codes, thus not allowing for any overhead saving, independently of the choice of boundary conditions.

### Error models

We perform quantum error correction with data and ancilla qubits placed in the same square array, analogous to an unrotated surface code. To measure a stabilizer, a CZ gate has to be applied between the ancilla qubit, located in the middle of the cross describing the

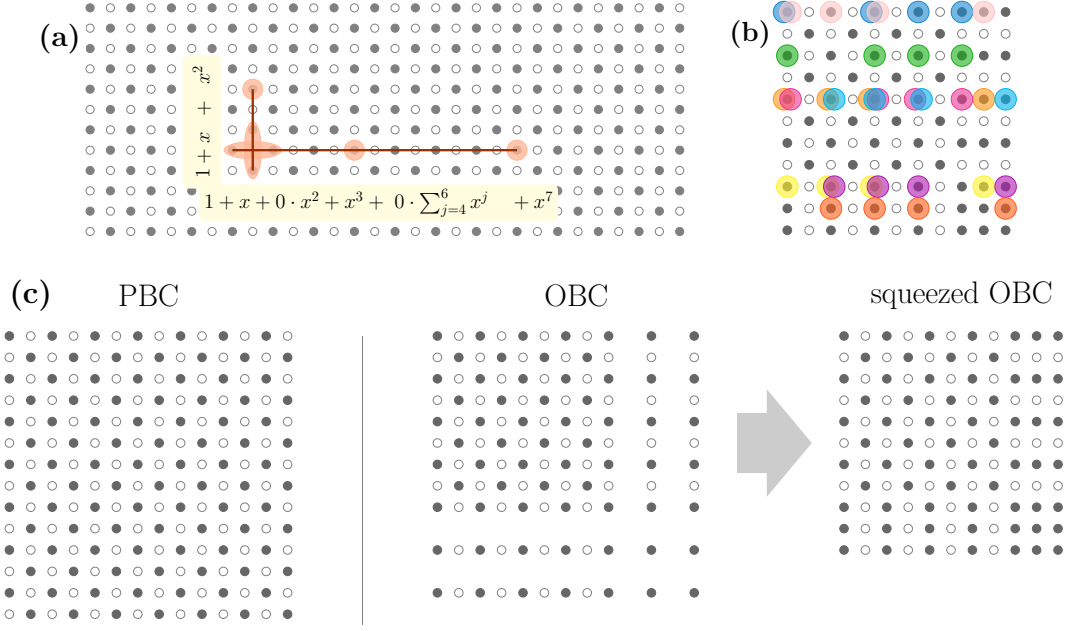


FIG. 2. (a) Classical polynomial seeds constraining stabilizer shape and ruling one lattice direction each. Both symmetric and asymmetric configurations are allowed. The examples here refer to the cases  $n_1 = 6$ ,  $k_1 = 2$  (vertical) and  $n_2 = 15$ ,  $k_2 = 7$  (horizontal). Data(ancilla) qubits are coloured black(white). (b) The  $[[65, 9, 4]]$   $k = 3$ -LDPC code with the 9 partially overlapping horizontal logical  $Z$  operators shown in different colors. (c) Array shape with periodic boundary conditions (PBC), open boundary conditions (OBC) and squeezed open boundary conditions, assuming  $n = 7$  and  $k = 3$  (equal seeds).

stabilizers, and the six data qubits [see Fig. 1(a/b)]. For the four data qubits which directly neighbor the ancilla qubits, this can be done simultaneously for all stabilizers [21], while the long-range CZ gates to the remaining data qubits have to be applied separately for  $X$  and  $Z$  stabilizers, leading to a stabilizer measurement circuit of depth 10 [see Fig. 1(b)].

The code tolerance against errors is probed via numerical simulations under circuit-level depolarizing noise, which is chosen to directly compare with existing literature [5, 7]. We assume uniformly distributed Pauli errors drawn from  $\{X, Z, Y\}$  and  $\{I, X, Z, Y\}^{\otimes 2} \setminus \{I \otimes I\}$  with probability  $p_1/3$  and  $p_2/15$  for single and two-qubit errors, respectively. We simulate  $D$  rounds of syndrome measurements, using Stim [22] to sample from the code circuit and Belief Propagation with Ordered Statistics Decoder (BP+OSD) [23, 24] to process syndrome information (see Methods). The latter is commonly regarded as one of the most viable approaches to decode arbitrary quantum LDPC codes.

For the error model above, we denote our error probabilities as  $\{p_1, p_2(j), p_p, p_m\}$  where  $p_1$  is the aforementioned single-qubit error probability,  $p_2(j)$  is the two-qubit error probability for separations of  $j$  in units of lattice spacing between control and target,  $p_p$  and  $p_m$  are the preparation and measurement error probabilities respectively. Idle errors are neglected. We focus most of our analysis on noise ratios appropriate for neutral atom

hardware based on numbers reported in experiments for state preparation and measurement (SPAM) errors [25], and gate errors [25, 26], by adopting the following *hardware-specific noise* parameters  $\{p = p_2(1), p_2(j) = c_j p, p_1 = p/10, p_p = p_m = 2p\}$ , with  $c_j$  the proportionality constants between long-range two-qubit gate error probabilities and the nearest neighbour two-qubit gate error probability (see below). The choice of linear dependence is justified in the Methods section. We note that, when squeezed open boundary conditions are enforced, long-range gates get shorter and the associated fidelities improve at the boundaries. Subsequently, anticipating potential implementation with other platforms, we provide numerical results for an *hardware-agnostic noise* parameter set using  $\{p \equiv p_1 = p_2(j) \forall j, p_p = p_m = 0\}$ , i.e. where all unitary gate errors are treated as equal while measurement and reset gates are perfect.

### Performance of La-cross codes

Overhead reduction against the surface code is the main motivation for adopting quantum LDPC codes. As shown in Fig. 1(c), the present code family offers a significant advantage in terms of encoding rate, and hence qubit overhead, when compared to surface codes having the same number of logical qubits and distance, although asymptotically both still scale like  $K = \mathcal{O}(1)$ ,  $D =$

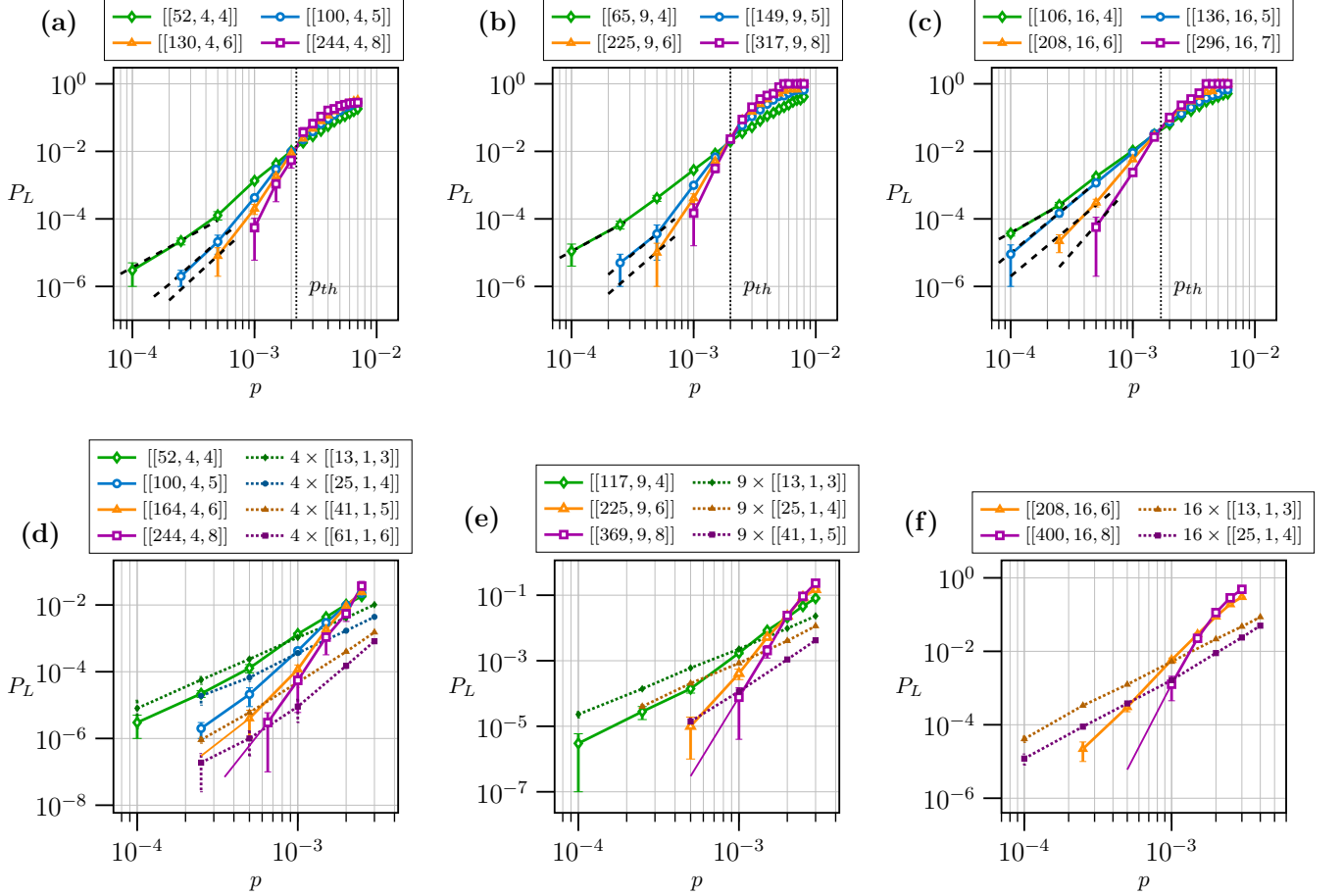


FIG. 3. Cumulative logical error probability normalized by the number,  $D$ , of rounds  $P_L(p) = (1 - p_L(p))^{1/D}$  for  $k = 2$  (a),  $k = 3$  (b),  $k = 4$  (c) vs nearest-neighbor two-qubit gate error probability  $p$ , under circuit-level depolarizing errors with hardware-specific noise. Error bars correspond to standard deviations  $\sigma_{P_L} = \sqrt{P_L(1 - P_L)/(\text{shots})}$ . Vertical dotted lines indicate the approximate location of the threshold probability  $p_{th}$ . Dashed black lines are added to show the qualitative good agreement of the decoding curves with the expected asymptotic scaling. (d)-(f) Logical error probability comparison against the surface code given same number of logical and physical qubits. For larger-distance codes extrapolations to lower logical error probabilities are shown (solid lines) to guide the eye. Surface code simulations have been performed under depolarizing noise with same single- and nearest neighbour two-qubit gate and SPAM errors as the LDPC codes.

$\mathcal{O}(\sqrt{N})$ . Along with overhead saving, the present code family also shows advantage over the surface code given equal number of physical and logical qubits, offering always larger code distance and lower logical error probability for sufficiently small physical error probabilities, as shown below.

In Fig. 3(a)-(c) we first present the error correction performance for several different sizes of La-cross codes under hardware-specific noise and defer the hardware-agnostic case to the Methods section (Fig. 6(a)-(c)). We plot the *cumulative* logical error probability, i.e. the probability that any of the  $K$  logical qubits fails, normalized by the number of rounds,  $P_L = 1 - (1 - p_L)^{1/D}$  vs the nearest-neighbor two-qubit gate error probability  $p$ , with  $p_L = \text{errors/shots}$ , for  $k = 2, 3, 4$ -LDPC codes. This is consistent with real experiments where one wants *all*

logical qubits to be protected at the same time. We find nearest-neighbor two-qubit gate error probability thresholds  $p_{th}^{k=2} \approx 0.22\%$ ,  $p_{th}^{k=3} \approx 0.20\%$ ,  $p_{th}^{k=4} \approx 0.17\%$ , which for simulations with hardware-agnostic noise further improve to  $p_{th}^{k=2} \approx 0.38\%$ ,  $p_{th}^{k=3} \approx 0.45\%$ ,  $p_{th}^{k=4} \approx 0.5\%$  (see Methods). While in the latter case  $p_{th}^k$  increases with the degree of non-locality  $k$ , in the hardware-specific case long-range gates get longer and thus more faulty (see below) and so  $p_{th}^k$  decreases with  $k$ . In all cases, the slope of the decoding curves is found to be consistent within good agreement (black dashed lines) with the expected behaviour in the deep sub-threshold regime:  $P_L(p) \approx A(p/p_{th})^{D_e}$ , being  $D_e = \lfloor \frac{D+1}{2} \rfloor$  the effective distance of the code, namely the length of the minimal physical error chain triggering a logical error.

We show in Fig. 3(d)-(f) comparisons of error correc-

tion performance for the  $k = 2, 3, 4$ -LDPC codes with the surface code with equal number of logical and physical qubits. We find that in all cases a crossing occurs between the LDPC and surface code decoding curves at a given nearest-neighbor gate error probability  $p^* \sim 10^{-3}$ , with the LDPC achieving lower logical errors for  $p < p^*$  [see also Fig. 1(d)-(e)]. The crossing value  $p^* \sim 10^{-3}$  is already within experimental reach, despite the penalty on long-range gates we have enforced.

We observe that  $p^*$  slowly decreases as the distance increases. In the sub-threshold regime, the logical error probability for both codes scales as  $P_L(p) \approx A(p/p_{th})^{D/2} = A(p/p_{th})^{\beta\sqrt{N}}$ , with  $\beta = \mathcal{O}(1)$  and  $A$  is the logical error probability extrapolated from the power-law behaviour up to the threshold. Defining the two  $k$  dependent values  $\beta_{sc} = (2\sqrt{2K})^{-1}$  and  $\beta_{ldpc}$ , with the former determined by partitioning the  $N$  physical qubits into  $K$  surface codes so the number of logical qubits are equal for both, a simple argument (see Methods) shows that

$$p^* = \left( \frac{(p_{th}^{sc})^{\beta_{sc}}}{(p_{th}^{ldpc})^{\beta_{ldpc}}} \right)^{\frac{1}{\beta_{sc} - \beta_{ldpc}}} \left[ \left( \frac{A_{ldpc}}{A_{sc}} \right)^{\frac{1}{\beta_{sc} - \beta_{ldpc}}} \right]^{\frac{1}{\sqrt{N}}}$$

Therefore, since  $\beta_{sc} < \beta_{ldpc}$  by construction and from data extrapolation  $0 < (A_{ldpc}/A_{sc}) < 1$ , we find that  $p^*$  decreases as the size  $N$  increases, but converges to a constant greater than zero asymptotically. This ensures that the LDPC codes *always* offer lower logical error probability for sufficiently small physical error probabilities with respect to the surface code, given the same number of logical and physical qubits.

### Implementation with neutral atom qubits

In the following we discuss the implementation of our family of La-cross LDPC codes on neutral atom quantum computers. For concreteness, we assume an array of  $^{137}\text{Cs}$  atoms with lattice spacing  $R$  and take  $|0\rangle = |6s_{1/2}, F=3, m_F=0\rangle$  and  $|1\rangle = |6s_{1/2}, F=4, m_F=0\rangle$ . To perform a CZ gate between two atoms with a separation of  $j$  lattice sites we couple the state  $|1\rangle$  to a Rydberg state  $|r_j\rangle = |n_j s\rangle$  using a two photon transition via the intermediate  $|7p_{1/2}\rangle$  state with effective Rabi frequency  $\Omega_j$ . We choose the laser phase  $\varphi(t)$  according to the time-optimal (TO) protocol [27] in order to minimize gate duration and Rydberg scattering. Note that we propose to use *different* principal quantum numbers  $n_j$  for different interatomic distances. Hereafter in this section the symbol  $n$  will refer to principal quantum numbers and not to classical code parameters.

The atoms interact via a dipole-dipole interaction, which for large atomic distances  $jR$  can be perturbatively treated as a van der Waals interaction  $\sum_j B_j |r_j r_j\rangle \langle r_j r_j|$ , where the interaction strength  $B_j$  scales as  $B_j \propto$

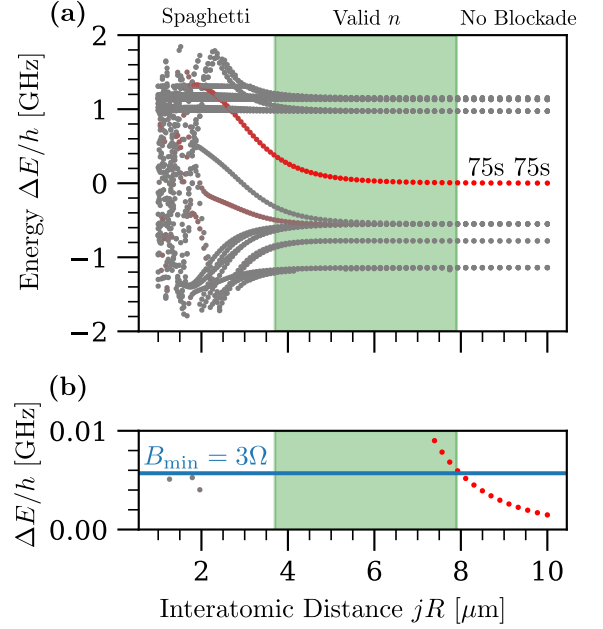


FIG. 4. Pair state interaction energy  $\Delta E$  calculated as a function of the interatomic distance  $jR$  for different eigenstates of the two-atom Hamiltonian. Red points are eigenenergies of eigenstates with the largest overlap with the  $|75s, 75s\rangle$  state. Panel (b) shows zoom-in of panel (a) on the range  $0 \leq \Delta E/h \leq 10$  MHz. Blue line shows the minimal interaction  $B = 3\Omega$  which we assume to be necessary for a Rydberg blockade gate (We take the realistic value  $\Omega = 2\pi \times 1.9$  MHz [13]) The range of valid distances in which there is a sufficient blockade ( $B \geq 3\Omega$ ) but we have not yet entered the “Spaghetti” regime, where the perturbative treatment of the dipole-dipole interaction between the atoms breaks down (see Methods), is shaded in green.

$n_j^{11}/(jR)^6$ . There are two constraints on our choice of  $n_j$ : First,  $n_j$  must be large enough to ensure a sufficient Rydberg blockade. While the TO protocol was originally designed in the limit  $B_j \gg \Omega_j$ , small variations of the phase profile  $\varphi(t)$  allow to implement a CZ gate as long as  $B_j \gtrsim \Omega_j$ . For concreteness, we here require  $B_j \geq 3\Omega_j$ , striking a compromise between allowing finite interaction strengths  $B_j$  while preserving the qualitative behavior of the  $B_j \gg \Omega_j$  limit. The second constraint is that  $n_j$  must be small enough such that the perturbative treatment of the dipole-dipole interaction is valid. For too large  $n_j$  we enter the so-called “Spaghetti” regime, in which the eigenstates of the two atom Hamiltonian cannot be approximated by product states anymore. Both the lower and the upper bound of  $n_j$  depend on the interatomic distance  $jR$ . This is exemplified in Fig. 4, which shows the eigenenergies of the two-atom Hamiltonian near the  $|75s, 75s\rangle$  state [28]. The shaded green area marks the range of interatomic distances  $jR$  for which  $n_j = 75$  allows for a sufficient Rydberg blockade without entering the “Spaghetti” regime.

For a realistic analysis of the logical error probability

it is crucial to understand how the physical error probability scales with the number of lattice sites  $j$  between the atoms. To estimate this, we assume that the only two sources of infidelity are the decay of the Rydberg states with decay rates  $\gamma_j$  and dephasing of the Rydberg states due to a Doppler shift arising from thermal motion of the atoms at  $T = 10 \mu\text{K}$ . The infidelity of a time-optimal CZ gate is then given by [29]

$$1 - F_j = 2.96 \frac{\gamma_j}{\Omega_j} + 7.12 \frac{\Delta_{\text{Doppler}}^2}{\Omega_j^2} \quad (1)$$

where  $\Delta_{\text{Doppler}} = k_{\text{eff}} \sqrt{k_B T / m}$  and  $k_{\text{eff}}$  is the effective wave vector of the two photon transition. To find the value  $n_j$  with the lowest infidelity  $1 - F_j$  we assume realistic values of  $R = 3 \mu\text{m}$  and  $1/\gamma = 430 \mu\text{s}$  at  $n = 75$  and use the scalings  $\Omega \propto n^{-3/2}$  and  $\gamma \propto n^{-3}$  [30]. For each  $j$  we now consider different values of the laser intensity (characterized by the value of  $\Omega$  at a reference principal quantum number  $n = 75$ ) and numerically minimize  $1 - F_j$  over  $n_j$ , constraining  $n_j$  to be large enough to achieve a sufficient blockade and small enough to not enter the ‘‘Spaghetti’’ regime (see Methods). We find that for each  $j$  the relationship  $1 - F_j \approx c_j(1 - F_1)$  holds, with the constant  $c_j$  increasing with  $j$ . This scaling forms the basis of our numerical simulation of the logical error probability.

We note that also the gate duration  $\tau$  increases with increasing interatomic distance  $j$ , scaling as  $\tau \propto (jR)^{18/25}$  (see Methods). With demonstrated gate durations around 250 ns for nearest neighbor atoms [26], a gate between atoms separated by  $j = 7$  lattice sites (the maximum considered above), could be implemented in approximately 1  $\mu\text{s}$ .

The implementation on Rydberg atoms dictates that different two-qubit gates can only be implemented in parallel when the qubit pairs are sufficiently separated, since otherwise an atom in the Rydberg state in one qubit pair might blockade an atom in another qubit pair. A safe option is to divide the lattice into a rectangular grid of square subregions each of size  $2(k+1) \times 2(k+1)$  and measure each subregion stabilizers, one by one, in parallel over the grid. This will enable measuring all the stabilizers in  $2(k+1)^2$  measurement rounds.

Finally, we mention that while the values of the  $c_j$  are specific for Cs atoms at 10  $\mu\text{K}$ , we expect qualitatively similar behavior for other atoms at other temperatures. Dephasing of the Rydberg state arising from sources other than Doppler shifts and optical pumping by black body radiation could be easily incorporated in our model by adding an additional term in Eq. (1). Additional dephasing errors would reduce the optimal principal quantum numbers  $n_j$ , while additional decay due to black body radiation would increase them. Other error sources, such as leakage to other states, would require a more elaborate error model. However, most error sources

become more detrimental with longer gate durations, and thus with larger interatomic distances. This is in accordance with our assumption that gate infidelities increase with  $j$ .

## DISCUSSION AND OUTLOOKS

We have developed an integrated approach to neutral atom QEC exploiting flexible data/ancilla qubit layout together with tunable long-range gates using multiple laser colors addressing distinct Rydberg states. Our analysis focuses on a sub-family of HGP quantum LDPC codes with high rate, low stabilizer weight, and moderate non-locality. All these features make them promising candidates to be implemented on near-term neutral atom quantum computers with all qubits in place. The limiting gate time is set by the slowest elementary gate, which is typically state preparation and measurement. Since all ancilla measurements can be deferred to the end of a round of stabilizers circuits, the overall time to perform a round of stabilizer measurements for La-cross codes, even using restricted parallelization, is notably shorter than using qubit shuttling.

We have examined the performance of these codes via numerical simulations under circuit-level depolarizing noise, which is a useful tool for benchmarking the code performance and making comparisons against the surface code. Noise models beyond depolarizing noise, appearing in many realistic situations, are expected to improve our results. For example, in Rydberg atom arrays it has been predicted that up to 98% of errors can be converted to erasure errors [31], implying much better scaling of the logical error rate with physical probability. Other noise biases [32, 33] can easily be incorporated into our construction in full analogy with the XZZX surface code [34]. We defer the problem of addressing these issues to future work.

Finally, while we have focused here on how to achieve long-lived quantum memory, quantum computation will require implementing fault-tolerant logical gates. Various proposals have been made to perform logical gates with LDPC codes including using non-destructive Pauli measurements assisted with non-local gates [6] and code switching to another stabilizer code like the surface code [7]. Recent work shows a way to perform a subset of Clifford gates transversally in HGP codes [35]. The La-cross codes with open boundaries are square but not symmetric HGP codes and some of those techniques could be used to allow for transversal gates even while maintaining restricted non-locality for both stabilizers and logical gates by trapping the atoms in a folded triangular configuration in a static plane.

## ACKNOWLEDGEMENTS

We gratefully acknowledge discussions with Shannon Whitlock. This research has received funding from the European Union’s Horizon 2020 research and innovation programme under the Marie Skłodowska-Curie project 955479 (MOQS), the Horizon Europe programme HORIZON-CL4-2021-DIGITAL-EMERGING-01-30 via the project 101070144 (EuRyQa) and from the French National Research Agency under the Investments of the Future Program projects ANR-21-ESRE-0032 (aQCess), ANR-22-CE47-0013-02 (CLIMAQS) and QuantEdu-France. G.K.B. acknowledges support from the Australian Research Council Centre of Excellence for Engineered Quantum Systems (Grant No. CE 170100009). Computing time was provided by the High-Performance Computing Center of the University of Strasbourg. Part of the computing resources were funded by the Equipex Equip@Meso project (Programme Investissements d’Avenir) and the CPER Alsacalcul/Big Data.

- 
- [1] A. Kitaev, Fault-tolerant quantum computation by anyons, *Annals of Physics* **303**, 2–30 (2003).
  - [2] E. Dennis, A. Kitaev, A. Landahl, and J. Preskill, Topological quantum memory, *Journal of Mathematical Physics* **43**, 4452–4505 (2002).
  - [3] N. P. Breuckmann and J. N. Eberhardt, Quantum low-density parity-check codes, *PRX Quantum* **2**, 10.1103/prxquantum.2.040101 (2021).
  - [4] D. Gottesman, Fault-tolerant quantum computation with constant overhead (2014), arXiv:1310.2984 [quant-ph].
  - [5] S. Bravyi, A. W. Cross, J. M. Gambetta, D. Maslov, P. Rall, and T. J. Yoder, High-threshold and low-overhead fault-tolerant quantum memory, *Nature* **627**, 778 (2024).
  - [6] L. Z. Cohen, I. H. Kim, S. D. Bartlett, and B. J. Brown, Low-overhead fault-tolerant quantum computing using long-range connectivity, *Science Advances* **8**, eabn1717 (2022), <https://www.science.org/doi/pdf/10.1126/sciadv.abn1717>.
  - [7] Q. Xu, J. P. B. Ataiades, C. A. Pattison, N. Raveendran, D. Bluvstein, J. Wurtz, B. Vasic, M. D. Lukin, L. Jiang, and H. Zhou, Constant-overhead fault-tolerant quantum computation with reconfigurable atom arrays (2023), arXiv:2308.08648 [quant-ph].
  - [8] J.-P. Tillich and G. Zemor, Quantum ldpc codes with positive rate and minimum distance proportional to the square root of the blocklength, *IEEE Transactions on Information Theory* **60**, 1193–1202 (2014).
  - [9] A. A. Kovalev and L. P. Pryadko, Improved quantum hypergraph-product ldpc codes, in *2012 IEEE International Symposium on Information Theory Proceedings* (IEEE, 2012).
  - [10] A. A. Kovalev and L. P. Pryadko, Quantum kronecker sum-product low-density parity-check codes with finite rate, *Physical Review A* **88**, 10.1103/physreva.88.012311 (2013).
  - [11] R. Wang and L. P. Pryadko, Distance bounds for generalized bicycle codes (2022), arXiv:2203.17216 [quant-ph].
  - [12] I. Bloch, J. Dalibard, and W. Zwerger, Many-body physics with ultracold gases, *Reviews of Modern Physics* **80**, 885–964 (2008).
  - [13] M. Saffman, T. G. Walker, and K. Mølmer, Quantum information with rydberg atoms, *Reviews of Modern Physics* **82**, 2313–2363 (2010).
  - [14] A. Browaeys and T. Lahaye, Many-body physics with individually controlled rydberg atoms, *Nature Physics* **16**, 132–142 (2020).
  - [15] L. Henriët, L. Beguin, A. Signoles, T. Lahaye, A. Browaeys, G.-O. Reymond, and C. Jurczak, Quantum computing with neutral atoms, *Quantum* **4**, 327 (2020).
  - [16] M. Morgado and S. Whitlock, Quantum simulation and computing with rydberg-interacting qubits, *AVS Quantum Science* **3**, 10.1116/5.0036562 (2021).
  - [17] D. Bluvstein, S. J. Evered, A. A. Geim, S. H. Li, H. Zhou, T. Manovitz, S. Ebadi, M. Cain, M. Kalinowski, D. Hangleiter, J. P. B. Ataiades, N. Maskara, I. Cong, X. Gao, P. S. Rodriguez, T. Karolyshyn, G. Semeghini, M. J. Gullans, M. Greiner, V. Vuletić, and M. D. Lukin, Logical quantum processor based on reconfigurable atom arrays, *Nature* 10.1038/s41586-023-06927-3 (2023).
  - [18] Y. Hong, M. Marinelli, A. M. Kaufman, and A. Lucas, Long-range-enhanced surface codes (2024), arXiv:2309.11719 [quant-ph].
  - [19] H. Bombin, I. H. Kim, D. Litinski, N. Nickerson, M. Pant, F. Pastawski, S. Roberts, and T. Rudolph, Interleaving: Modular architectures for fault-tolerant photonic quantum computing (2021), arXiv:2103.08612 [quant-ph].
  - [20] S. Jandura, V. Srivastava, L. Pecorari, G. Brennen, and G. Pupillo, Non-local multi-qubit quantum gates via a driven cavity (2023), arXiv:2303.13127 [quant-ph].
  - [21] Y. Tomita and K. M. Svore, Low-distance surface codes under realistic quantum noise, *Physical Review A* **90**, 10.1103/physreva.90.062320 (2014).
  - [22] C. Gidney, Stim: a fast stabilizer circuit simulator, *Quantum* **5**, 497 (2021).
  - [23] J. Roffe, D. R. White, S. Burton, and E. Campbell, Decoding across the quantum low-density parity-check code landscape, *Physical Review Research* **2**, 10.1103/physrevresearch.2.043423 (2020).
  - [24] J. Roffe, LDPC: Python tools for low density parity check codes (2022).
  - [25] T. M. Graham, Y. Song, J. Scott, C. Poole, L. Phuttitarn, K. Jooya, P. Eichler, X. Jiang, A. Marra, B. Grinkemeyer, M. Kwon, M. Ebert, J. Cherek, M. T. Lichtman, M. Gillette, J. Gilbert, D. Bowman, T. Ballance, C. Campbell, E. D. Dahl, O. Crawford, N. S. Blunt, B. Rogers, T. Noel, and M. Saffman, Multi-qubit entanglement and algorithms on a neutral-atom quantum computer, *Nature* **604**, 457–462 (2022).
  - [26] S. J. Evered, D. Bluvstein, M. Kalinowski, S. Ebadi, T. Manovitz, H. Zhou, S. H. Li, A. A. Geim, T. T. Wang, N. Maskara, H. Levine, G. Semeghini, M. Greiner, V. Vuletić, and M. D. Lukin, High-fidelity parallel entangling gates on a neutral-atom quantum computer, *Nature* **622**, 268–272 (2023).
  - [27] S. Jandura and G. Pupillo, Time-optimal two- and three-qubit gates for rydberg atoms, *Quantum* **6**, 712 (2022).
  - [28] N. Šibalić, J. Pritchard, C. Adams, and K. Weatherill, Arc: An open-source library for calculating properties of alkali rydberg atoms, *Computer Physics Communica-*

- tions **220**, 319–331 (2017).
- [29] S. Jandura, J. D. Thompson, and G. Pupillo, Optimizing rydberg gates for logical-qubit performance, *PRX Quantum* **4**, 020336 (2023).
  - [30] T. F. Gallagher, Rydberg atoms, *Reports on Progress in Physics* **51**, 143 (1988).
  - [31] Y. Wu, S. Kolkowitz, S. Puri, and J. D. Thompson, Erasure conversion for fault-tolerant quantum computing in alkaline earth rydberg atom arrays, *Nature Communications* **13**, 10.1038/s41467-022-32094-6 (2022).
  - [32] J. Roffe, L. Z. Cohen, A. O. Quintavalle, D. Chandra, and E. T. Campbell, Bias-tailored quantum ldpc codes, *Quantum* **7**, 1005 (2023).
  - [33] A. Dua, A. Kubica, L. Jiang, S. T. Flammia, and M. J. Gullans, Clifford-deformed surface codes, *PRX Quantum* **5**, 10.1103/prxquantum.5.010347 (2024).
  - [34] J. P. Bonilla Ataides, D. K. Tuckett, S. D. Bartlett, S. T. Flammia, and B. J. Brown, The xxx surface code, *Nature Communications* **12**, 10.1038/s41467-021-22274-1 (2021).
  - [35] A. O. Quintavalle, P. Webster, and M. Vasmer, Partitioning qubits in hypergraph product codes to implement logical gates, *Quantum* **7**, 1153 (2023).
  - [36] T. M. Graham, M. Kwon, B. Grinkemeyer, Z. Marra, X. Jiang, M. T. Lichtman, Y. Sun, M. Ebert, and M. Saffman, Rydberg-mediated entanglement in a two-dimensional neutral atom qubit array, *Phys. Rev. Lett.* **123**, 230501 (2019).

## METHODS

### Quantum error correction simulations

In the following we provide further detail about quantum error correction simulations. The qubit register is firstly initialized to  $|0\rangle$ , Hadamard gates are acted on  $X$ -type ancilla qubits and subsequent CNOT gates are applied according to the order prescription specified in the main text (Fig. 1(a),(b)). We simulate as many rounds of syndrome measurements as the code distance, with ancilla measurement and reset after any round and data measurement occurring only after the last round. State preparation and measurement bit-flip errors and single- and two-qubit gate depolarizing errors are applied with probabilities specified in the main text, under both hardware-specific and agnostic noise model, which we show here in Fig. 6. Idle errors are always neglected.

Belief Propagation with Ordered Statistics Decoder (BP+OSD) [23, 24] has been used to obtain all the decoding plots shown in the main text. We have optimized over the decoder parameters and opted for the minimum-sum variant of Belief Propagation with a scaling factor of  $s = 1.0$  for all LDPC codes. The number of iterations of Belief Propagation was found to be almost irrelevant, so we have fixed it to 4. Ordered Statistics Decoding was performed in combination sweep mode up to order 1 to speed up the decoding process, upon testing up to order 10 without finding any relevant improvement. Monte

Carlo samplings have been performed using the Sinter library with  $10^3$  decoder maximal number of errors cutoff and increasing maximal number of samples cutoff with decreasing physical error rate,  $\sim 10^4 - 10^7$ , compatibly with the system sizes.

Surface code simulations are performed under the same noise model of the LDPC codes they are compared to, performing  $D_{\text{ldpc}}$  rounds of stabilizer measurements so to keep qubits alive for the same amount of time for both codes. Logical error probability is computed as  $P_L(p) = 1 - (1 - P_L^1(p))^K$ , being  $P_L^1(p)$  the single surface code logical error probability. For the fairest comparison, we want to compare our (LDPC code, BP+OSD decoder)-pair against the surface code with its best decoder. Given the impractically huge time overhead of the maximum-likelihood decoder, we have opted for decoding the surface code with the BP+OSD decoder with optimized scaling factor  $s = 0.625$ , which was found to outperform the minimum-weight perfect matching decoder with open boundaries. Thus, with safe confidence, we claim that our comparing argument can only benefit from better decoders for the LDPC codes.

### Analytical sub-threshold error estimation

The crossing point between LDPC and surface code decoding curves,  $p^*$ , given equal number of logical and physical qubits decreases as the distance increases. We can provide a quantitative and decoder-independent estimate of this behaviour via the following analytical argument. In the sub-threshold regime, the logical error probability scales as

$$P_L(p) \approx A \left( \frac{p}{p_{th}} \right)^{\alpha D} = A \left( \frac{p}{p_{th}} \right)^{\beta \sqrt{N}} \quad (2)$$

with  $\alpha = 1/2$  asymptotically and  $\beta = \mathcal{O}(1)$  being code dependent. For either code, the distance as a function of  $N$  can be computed from

$$N = (\lambda_k D_{\text{ldpc}} - k)^2 + (\lambda_k D_{\text{ldpc}})^2 \approx 2\lambda_k^2 D_{\text{ldpc}}^2 \quad (3)$$

$$N = K((D_{\text{sc}} - 1)^2 + D_{\text{sc}}^2) \approx 2KD_{\text{sc}}^2$$

being  $\lambda_k$  some constant depending on the order  $k$  of the LDPC code, for which – we recall – the code distance is  $D = \mathcal{O}(\sqrt{N})$  and  $K$  constant for a given code. The crossing rate can be computed by requiring

$$A_{\text{sc}} \left( \frac{p^*}{p_{th}^{\text{sc}}} \right)^{\beta_{\text{sc}} \sqrt{N}} \stackrel{!}{=} A_{\text{ldpc}} \left( \frac{p^*}{p_{th}^{\text{ldpc}}} \right)^{\beta_{\text{ldpc}} \sqrt{N}}, \quad (4)$$

leading to

$$p^* = \left( \frac{(p_{th}^{\text{sc}})^{\beta_{\text{sc}}}}{(p_{th}^{\text{ldpc}})^{\beta_{\text{ldpc}}}} \right)^{\frac{1}{\beta_{\text{sc}} - \beta_{\text{ldpc}}}} \left[ \left( \frac{A_{\text{ldpc}}}{A_{\text{sc}}} \right)^{\frac{1}{\beta_{\text{sc}} - \beta_{\text{ldpc}}}} \right]^{\frac{1}{\sqrt{N}}}. \quad (5)$$

Therefore, when  $0 < (A_{\text{ldpc}}/A_{\text{sc}})^{1/(\beta_{\text{sc}}-\beta_{\text{ldpc}})} < 1$  the crossing point decreases with  $N$  for  $\beta_{\text{sc}} < \beta_{\text{ldpc}}$ , which is always our case by construction.

### Realistic Infidelity Calculations

In the following we detail our estimate of the gate error for an implementation on Rydberg atoms. For a given interatomic distance  $jR$  and a given laser intensity, characterized by the Rabi frequency  $\Omega$  at a fixed reference  $n$ , e.g.  $n = 75$ , we proceed as follows: We first use the AtomicRydbergCalculator (ARC) [28] to determine the lowest  $n_j$  for which we still obtain  $B_j \geq 3\Omega_j$  (note that both  $B_j$  and  $\Omega_j$  change with  $n_j$ ), as well as the highest  $n_j$  which is admissible without entering the Spaghetti regime. We define the start of the Spaghetti regime as the smallest value of  $n_j$  for which there is an eigenstate of the two-atom Hamiltonian which has a smaller pair state interaction energy  $|\Delta E|$  than the perturbed  $|75s, 75s\rangle$  state. We only consider states with a non-zero dipole-dipole

coupling to the intermediate  $|7p_{1/2}\rangle$  state in this comparison.

Having established the upper and the lower bound of  $n_j$ , we then minimize the infidelity  $1 - F_j$  [Eq. (1)] over this range. Fig. 5(a) shows an example of this for an interatomic distance of  $jR = 9 \mu\text{m}$  with a laser intensity such that at  $n = 75$  we have  $\Omega = 2\pi \times 1.9 \text{ MHz}$  [36]. In this example, as in all cases considered by us, the lowest infidelity is achieved at the lower bound of the allowed values of  $n$ .

In Fig. 5 we vary the Rabi frequency  $\Omega$  at  $n = 75$  from  $2\pi \times 0.5 \text{ MHz}$  to  $2\pi \times 15 \text{ MHz}$  and compare the gate error  $1 - F_j$  for gates over  $j$  lattice sites as a function of gate error  $1 - F_1$  for nearest neighbor gates. The ratios  $c_j = (1 - F_j)/(1 - F_1)$  are approximately independent of  $\Omega$  and given by  $c_1 = 1$ ,  $c_2 \approx 1.6$ ,  $c_3 \approx 2.5$ ,  $c_4 \approx 3.6$ ,  $c_5 \approx 4.8$ ,  $c_6 \approx 6.1$ ,  $c_7 \approx 7.5$ .

Since the lowest fidelity is always achieved by the lowest value of  $n$  which still gives a sufficient blockade, the ratio  $B/\Omega \propto n^{25/2}/(jR)^6$  is constant, so that the optimal  $n$  scales as  $n_j \propto (jR)^{12/25}$ . The pulse duration then scales as  $\tau \propto \Omega^{-1} \propto n^{3/2} \propto (jR)^{18/25}$ .

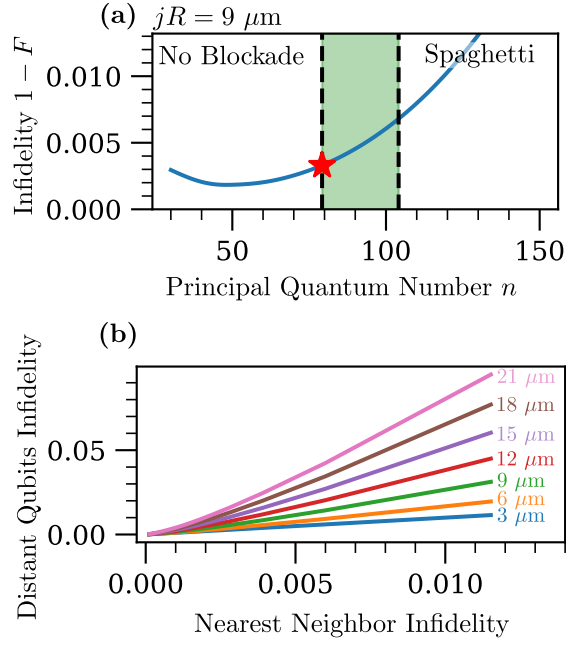


FIG. 5. (a) Infidelity for a CZ gate between two Cs atoms at  $jR = 9 \mu\text{m}$  as a function of the principle quantum number  $n_j$  (blue line). The shaded green area shows the allowed values if  $n_j$  in which there is a sufficient Rydberg blockade but we have not yet entered the Spaghetti regime. Red star shows the minimal infidelity for valid  $n_j$ , which is achieved at the lowest possible  $n_j$  allowing for a sufficient Rydberg blockade. (b) The infidelity of a CZ gate at interatomic distances between  $3 \mu\text{m}$  and  $21 \mu\text{m}$  ( $1 \leq j \leq 7$ ) as a function of the nearest neighbor infidelity (distance  $3 \mu\text{m}$ ).

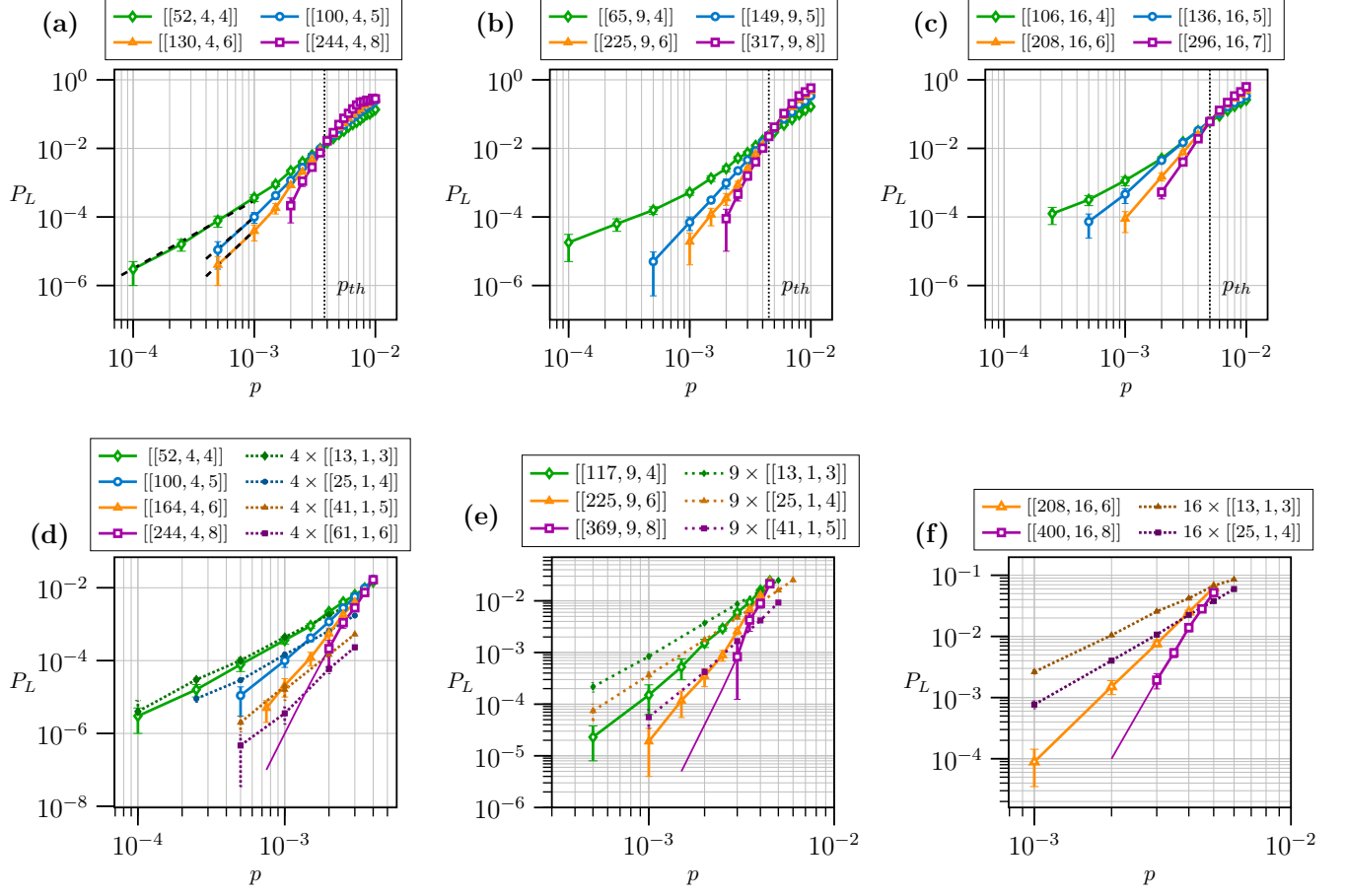


FIG. 6. Cumulative logical error probability normalized by the number,  $D$ , of rounds  $P_L(p) = (1 - p_L(p))^{1/D}$  for  $k = 2$  (a),  $k = 3$  (b),  $k = 4$  (c) under circuit-level depolarizing errors with hardware-agnostic noise. Error bars correspond to standard deviations  $\sigma_{P_L} = \sqrt{P_L(1 - P_L)/(\text{shots})}$ . Vertical dotted lines indicate the approximate location of the threshold probability  $p_{th}$ . For  $k = 2$  only, dashed black lines are added to show the qualitative good agreement of the decoding curves with the expected asymptotic scaling. (d)-(f) Logical error probability comparison against the surface code given same number of logical and physical qubits. Surface code simulations have been performed under depolarizing noise with the same error model of LDPC codes.